Application of Monte Carlo simulation methods to quantum cosmology

Beverly K. Berger*
Physics Department, Oakland University, Rochester, Michigan 48309
(Received 25 February 1993)

Quantum Monte Carlo (MC) simulation methods used widely throughout physics to generate ground-state wave functions are applied to the minisuperspace quantization of spatially homogeneous cosmologies. MC diffusion, MC path integral, and semiclassical MC path integral methods are applied to the de Sitter model, the mixmaster universe (and its generalizations), and the Robertson-Walker scalar field cosmology. All methods adequately reproduce the de Sitter model's wave function in the regime that has an effective ground state. In other situations, the failure of the Hamiltonian constraint (i.e., Wheeler-DeWitt operator) to be bounded from below presents a severe obstacle to the simulations. If a ground state is artificially forced, the various MC methods can be compared in more complicated models. The simulations can then be used to study issues such as the validity of the minisuperspace approximation, the choice of a time variable, the path space measure, and tunneling universe wave functions.

PACS number(s): 98.80.Bp, 04.60.+n

I. INTRODUCTION

The observed Universe on the largest scales can be understood as a Friedmann-Robertson-Walker (FRW) spatially homogeneous, isotropic collisionless matter-filled solution to Einstein's equations. Observations of the cosmic microwave background (CMB) and light element abundances yield information about earlier radiation-dominated and nucleosynthesis eras, respectively. Recent observations from the Cosmic Background Explorer (COBE) of CMB fluctuations [1] may allow the study of even earlier epochs associated with the properties of grand unified theories. Yet, at some point in the past direction, the FRW model must break down since it is expected that Einstein's equations are no longer valid at energies (or equivalently temperatures) above the Planck scale. Even if hidden to the past of an inflationary era, one expects that an era of quantum gravitational effects will have occurred. (It is also possible to consider a more speculative scenario in which the Universe itself is always a quantum system with the classical world a creature of the measurement process [2].) Unfortunately, no complete theory of quantized gravitation yet exits. To allow concrete study of possible effects in this regime, it has often been useful to consider the better-defined quantum mechanics of spatially homogeneous cosmologies [3]. Here we regard a spatially homogeneous cosmology to be a finite degree of freedom (DF) dynamical system in its own right. Quantum cosmology (QC) is defined here to be the quantum mechanics of these systems. The important technical advantage of QC over the quantum mechanics of the gravitational field (QG) is that the complications of quantum field theory may be neglected. The construction of a framework for QC is still nontrivial, however, because many of the standard QG problems associated with the time DF remain in the truncated QC paradigm [4].

As is well known [5,6], there is no guarantee that the properties of a QC solution bear any relationship to those of a QG that (classically) contains the QC since DF's have been eliminated in violation of the uncertainty principle. Recent studies of the validity of the QC "approximation" indicate (not unexpectedly) that the QC results cannot be trusted if there is significant mixing between the retained and neglected modes of the full QG theory [7]. Nonetheless, the QC model serves a useful function both as a theoretical laboratory, particularly for the study of issues related to the choice of time variable, and as a tractable system within which examples of possible quantum effects in the early Universe might be constructed.

Even within QC, systems with several DF's cannot be solved analytically (although a semiclassical analysis can be used as was done in, e.g., Refs. [8–11]). Certainly as a prelude to QG, appropriate numerical methods must be sought. A fruitful methodology used throughout physics to study complicated many DF systems is quantum Monte Carlo (MC) simulation [12]. For example, in MC path-integral (PI) simulations [13,14], the Feynman PI formulation of quantum mechanics [15] is used to construct the quantum propagator (schematically) as

$$K \approx \sum_{\text{paths}} \exp(iS) , \tag{1.1}$$

where S is the (Lorentzian) action for the system. Boundary conditions are implemented by the choice of paths (in the dynamical configuration space of the system) over which the (formal) sum is to be taken. Schematically, one formulation of an MCPI simulation [12] has a procedure to select discretized paths in the configuration space and to determine their contribution to the propagator using

*Electronic address: berger@vela.acs.oakland.edu

$\exp(-S_E)$ (where S_E is the Wick rotated Euclidean action) to weight the paths. The actual algorithm must also be constructed to correctly reproduce the path space measure.

Application of quantum MC methods to QC is not straightforward because the appropriate Euclidean action (equivalent to some multiple of the integrated Hamiltonian constraint of general relativity) is not generically bounded from below. This is due to the Lorentzian signature of the (mini)superspace (MSS) metric [6] and the fact that the spatial scalar curvature can be arbitrarily negative. If the quantum theory is taken to be the Wheeler-DeWitt (WD) equation [6]

$$\hat{\mathcal{H}}\Psi=0 \tag{1.2}$$

(where $\hat{\mathcal{H}}$ is the operator form of the Hamiltonian constraint and Ψ is the wave function of the Universe), we see the additional problem that, regarded as a formal Schrödinger equation in coordinate time, the solution at zero energy is not (necessarily) a ground state. Although proposals to solve (or at least correctly bypass) this dilemma have been made, with several under active consideration in the numerical simulations [16–19], it cannot yet be said that the problem has been solved. Here we report the results of a series of studies using an artificial *Ansatz* to force the system to be well defined (see also Refs. [20–23]). Within this *Ansatz* (i.e., although one cannot directly reproduce solutions to the WD equations) comparisons of models with regard to path space measure, choice of time variable, and DF's included in the model can be made. The essence of the *Ansatz* (for MCPI simulations) is to consider in some way the absolute value of Hamiltonian constraint [20]. The qualitative results (e.g., the shape of the wave function) do not depend on the precise form of the *Ansatz*.

In Sec. II we shall describe the problem we are trying to solve—to obtain the wave function in MSS (the finite-dimensional configuration space for the dynamics of the spatially homogeneous cosmology). In Sec. III, examples of simulation methods with their strengths and weaknesses shall be given. Section IV will contain a comparison among several methods for the de Sitter model used as an example in many studies. We shall see that most methods can correctly reproduce the exact solution in the regime where there is an effective ground state. Section V will contain similar comparisons for the more complicated mixmaster (vacuum, diagonal, Bianchi-type IX) universe. Here we shall see that different methods yield qualitatively different results. Section VI will contain examples of studies of path space measure (the Arnowitt-Deser-Misner [24] (ADM) reduction), choice of time variable (the Wald-Unruh proposal [25]), tunneling origin of the Universe (in the de Sitter model) (see, for example, Refs. [11,26]), and the validity of the MSS approximation (scalar field coupled to mixmaster) [7,23]. Section VII will contain a summary and a discussion of future directions.

II. THE WAVE FUNCTION IN MINISUPERSPACE

For the class A spatially homogeneous cosmologies [27], the complete set of Einstein's equations may be obtained by variation of αH where $\alpha(t)$ is the lapse function and H is the (integrated) Hamiltonian constraint. In general, for these models, one can transform from the metric to some convenient set of variables $\{q^A\}$, $A=0,\ldots,N-1$ that describe the N DF's of the Universe. In terms of the q^A and their conjugate momenta p_A after rescaling the lapse via $\alpha=\sqrt{g}$ (with g the determinant of the induced metric on the spacelike hypersurfaces determined by homogeneity), H typically takes the form [28] (where $\hbar=c=16\pi G=1$)

$$H=G^{AB}(q)p_A p_B+V(q)\ . \tag{2.1}$$

Here G_{AB} is the Lorentzian MSS metric while $V(q)={}^3R$ for ${}^3R$ the spatial scalar curvature. The reduction to MSS of the Dirac method for canonical quantization of constrained systems leads to the WD equation [6]

$$\hat{H}\left[q^A, p_A\rightarrow -i\frac{\partial}{\partial q^A}\right]\Psi(q^A)=0\ , \tag{2.2}$$

where $\hat{H}$ is the operator form of (2.1) and $\Psi(q^A)$ is the wave function on the MSS with axes $\{q^A\}$. Here we shall note the following features of (2.2).

(1) Even in MSS, classical general relativity is invariant under a time reparametrization [4]. (The foliation of the spacetime has been fixed by the requirements of spatial homogeneity.) This means that one of the DF's of the system is not dynamical but is used up by the time variable [24]. This is the MSS projection of the more general, severe problems for quantization of gravity due to the arbitrariness of time in the classical theory. Extensive discussion of these issues appears in the literature [4].

(2) The interpretation of the wave function is problematical since the standard formalism presupposes an external (classical) measuring apparatus. Extensive work has been performed to develop a modification of the usual interpretation of quantum mechanics to allow its application to the Universe as a single self-contained quantum system [2]. This work has the further goal to explain the classical macroscopic world as a manifestation of decoherence that is inevitable in our interactions with the rest of the quantum Universe. Here we shall assume that an acceptable interpretation of $\Psi(q^A)$ exists so that (2.2) is meaningful.

(3) The formal appearance of the WD equation as a zero energy Schrödinger equation suggests that the Universe is in its ground state [8]. It further implies that standard numerical simulation methods used to find ground states of quantum systems might be applied to QC [20]. Unfortunately, the WD operator $\hat{H}$ is not, in general, bounded from below due both to the Lorentzian signature of the MSS metric and to the fact that the spatial scalar curvature may be arbitrarily negative. The actual structure of (2.2) is therefore that of a Klein-Gordon equation on MSS. This has led to proposals for third quantization [29].

(4) One needs more than a differential equation to obtain the wave function of the Universe; boundary conditions are required [8,30]. As originally emphasized by Hartle and Hawking [8], other areas of physics impose

boundary conditions consistent with experience. For the wave function of the Universe, the boundary (actually initial) conditions must be imposed beyond the realm of possible experiment. Hartle and Hawking therefore proposed one (among many later proposed by others) of the possible boundary-condition formulations. For example, Hartle and Hawking proposed to restrict the wave function expressed as a PI: The amplitude for a given three-geometry is to be obtained as the sum over regular Euclidean four-geometries bounded by that three-geometry. In the trivial single DF de Sitter model with scale factor a, this condition selects a solution that is real at large a and exponentially decreasing toward $a \to 0$. Alternatively, one might consider Vilenkin's boundary condition [11] that there be no incoming radiation at the boundary of superspace. In the de Sitter model, this condition chooses the solution that has the form of a traveling wave at large a while exponentially increasing toward $a \to 0$ (so that it tunnels through the barrier between the two regions). Many other boundary-condition proposals have been made [31,32]. Unfortunately, the application of all these boundary conditions to models with many DF's is nontrivial and may be problematical [33].

(5) At a more technical level, the quadratic form of the momentum dependence of the Hamiltonian constraint with q-dependent coefficients causes essentially unresolvable factor ordering problems [4,34]. It is possible to interpret any factor ordering as that defined for a particular choice of variables with a q-independent MSS metric [28].

It is often possible (for popular models) to further simplify (2.1) by choosing variables for which the MSS metric is flat [28]. (This is a subset of the process of imposition of a particular factor ordering.) For the Bianchi-type cosmologies, this can be achieved by the variable choice $\{\Omega,\beta_+,\beta_-\}$ leading to a Hamiltonian constraint

$$2H=-p_\Omega^2+p_+^2+p_-^2+\zeta e^{4\Omega}V(\beta_+,\beta_-)\ , \tag{2.3}$$

where ζ is an arbitrary constant.

Simulations often require the Feynman PI (here given conveniently for a single DF) denoted schematically by [15,35]

$$\langle q,t|q',t'\rangle=\int \mathcal{D}[q(t)]\exp(iS)\ , \tag{2.4}$$

where $\mathcal{D}[q(t)]$ is the measure in the space of all paths which start at $q'(t')$ and end at $q(t)$ and

$$S=\int_{t'}^{t} dt''\, L(q,\dot{q},t'') \tag{2.5}$$

is the action for the Lagrangian L. The wave function may be found from (2.4) with the standard expression [15]

$$\psi(q,t)=\int dq'\langle q,t|q',t'\rangle\psi(q',t') \tag{2.6}$$

so that (2.4) is the expression for the propagator. The relevance of the PI to numerical simulations arises from the following properties [15,28].

(1) If a quantum system (with a single DF for convenience) possesses a ground state with energy E_0 and a complete set of states $\varphi_N(q)$ with energies E_N, $N=0,\ldots,\infty$, then, in Euclidean time $\tau=it$,

$$|\varphi_0(q)|^2=\lim_{\tau\to\infty}\langle q,\tau|q,0\rangle\cdot \tag{2.7}$$

using (2.4) since, for this system,

$$\langle q,\tau|q,0\rangle=\sum_{N=0}^{\infty}\varphi_N^*(q)\varphi_N(q)e^{-E_N\tau}\ . \tag{2.8}$$

(2) The PI for this simple system can also be found directly in a discrete (skeletonized) form as [for, e.g., the Euclidean phase space form of (2.4)] with the measure given by

$$\mathcal{D}[q(\tau)]=\lim_{\substack{n\to\infty\\ \Delta\tau\to 0}}(2\pi)^{-2n}\prod_{k=1}^{n}dp_k\prod_{j=1}^{n-1}dq_j \tag{2.9}$$

and the action by

$$S_E=\sum_{k=1}^{n}\{p_k(q^k-q^{k-1})-\Delta\tau[\tfrac{1}{2}p_k^2-V(q^{k-1})]\}\ . \tag{2.10}$$

The Gaussian integrations over momenta can be performed to yield the Lagrangian form [15]

$$\langle q,\tau|q',0\rangle=\lim_{\substack{n\to\infty\\ \Delta\tau\to 0}}(2\pi)^{-n/2}\int\prod_{j=1}^{n-1}dq_j\exp\left[-\frac{(q^j-q^{j-1})^2}{2\Delta\tau}-\Delta\tau\,V(q^{j-1})\right]\ . \tag{2.11}$$

Expression (2.11) is easy to simulate on the computer [13,14,20]. One constructs a discrete path with points $q_i(\tau_j)$ subject to the appropriate boundary conditions. The path weight is just the integrand in (2.11) easily found from the path points. The integral $\prod dq$ is found by summing over many paths using some algorithm to yield the correct measure in path space. (Other schemes work directly with the Euclideanized Schrödinger equation regarded to be a diffusion equation [22,36].)

Of course, the time reparametrization invariance in the Hamiltonian constraint requires a modification of the PI since one DF is nondynamical [4,28,35,37]. The path integral must include integration over the lapse and takes the schematic (e.g., Lorentzian) form

$$\langle q^A,t|q'^A,0\rangle=\lim_{n\to\infty}\int d\alpha\, d^n p\, d^n q\exp\left[i\int dt\left[p_A\frac{dq^A}{dt}-\alpha H\right]\right]\ , \tag{2.12}$$

where H is given by (2.1) for a flat MSS. It is clear that the α integration yields (to the extent that anything is defined) a δ functional of the Hamiltonian constraint. The addition, e.g., of ghost fields to enforce some gauge condition can lead to a Faddeev-Popov determinant (for quantum mechanics rather than quantum field theory) which, in effect, implements the ADM reduction in the path integral. Alternatively, one may just fix the lapse to impose $\dot{\alpha}=0$ as a gauge condition. Extensive discussion (though not real resolution) of these matters is given in the literature [4,28,35,37,38].

In most of the following we shall fix the lapse and regard the Hamiltonian constraint to be a true Hamiltonian (albeit with "wrong" signs). We shall give one example [28] of a measure choice to yield the ADM reduction for the de Sitter model containing a conformally coupled scalar field. The momentum and lapse integrals may be performed for the ADM measure with intrinsic time gauge condition $q^0=\tau$ to yield (schematically)

$$\langle q^A|q^A\rangle=\lim_{n\to\infty}\prod\pi^{N/2}\Delta\tau\int\left[\frac{V^{1/2}(q^A)}{ds}\right]^{N/2}\times K_{N/2}(2V^{1/2}ds)\ , \quad (2.13)$$

where V is the potential term in the action (2.1), K is a modified Bessel function, and ds is MSS proper time for a system with N DF's. To simulate this model we need only weight the paths with the unusual expression in (2.13) rather than that in (2.11).

III. SIMULATION METHODS

Here we shall describe three major methods widely used in other areas of physics to obtain ground-state wave functions. We shall consider their operation in a well-behaved single DF quantum system described by a Euclidean action of the form (2.10). We shall then outline for each method how it might be made to apply to a system described by the Hamiltonian constraint (2.1).

A. Monte Carlo diffusion (MCD) [36,22,39]

In Euclidean time $\tau=it$, Schrödinger's equation becomes the diffusion equation

$$\frac{\partial\psi}{\partial\tau}(q,\tau)=\tfrac{1}{2}\nabla^2\psi(q,\tau)-V(q)\psi(q,\tau)\ . \quad (3.1)$$

If (3.1) is regarded to be in differential form (i.e., $\partial\tau\to\Delta\tau$), multiplication by $\Delta\tau$ yields a stochastic equation. The wave function $\psi(q,\tau)$ becomes the (necessarily non-negative) density of fictitious probability particles (*psips*). In the absence of the potential term, the diffusion equation is simulated as follows: Some initial number of *psips* is started at the origin with each undergoing a random walk with stepsize $\Delta x\propto(\Delta\tau)^{1/2}$. [Actually one allows the stepsize to be drawn from a Gaussian random distribution with zero mean and standard deviation $(\Delta\tau)^{1/2}$.] The potential $V(q)$ is treated as a source term creating or destroying *psips* according to a probability $\propto[V(q)-V_{\rm ref}]\Delta\tau$ (where $V_{\rm ref}$ is chosen to keep the *psip* number constant). The idea is that if the *psip* is located at a q such that $V(q)>V_{\rm ref}$, it is likely that the *psip* will be destroyed. If $V(q)<V_{\rm ref}$ an additional *psip* will probably be created at that location. Throughout the simulation, the time step is regularly decreased to obtain greater resolution in the *psip* distribution. As $\tau\to\infty$, the *psip* distribution yields $|\psi_0(q)|$. It is possible to obtain excited states by restricting the simulation to a range in q with nodes at the boundary—e.g., if $V(q)$ is even in q, the first excited state can be found by requiring a *psip* to be destroyed if it has $q\le 0$. Extension to more DF's is straightforward.

This method is very easy to use although its advantage over MCPI methods (discussed next) is not apparent for larger numbers of DF's. MCD has obvious disadvantages in its application to QC. There appears to be no obvious way to implement the Lorentzian signature of the MSS metric by some sort of antidiffusion in one direction. The only realistic option appears to be conformal rotation [40]. Furthermore, if the potential V has a "hole," i.e., if it can be arbitrarily negative for some value of q, the *psips* will fall into the hole. One can in an *ad hoc* manner avoid this problem (which is common in popular cosmological models) by taking $|V(q)|$. Examples will be given later. The nature of the rule for destroying *psips* at $V=\infty$ walls leads to an ability of MCD to handle potentials such as the infinite square well correctly.

B. Monte Carlo path integral (MCPI) [13,14,20,21]

MCPI appears to be among the most widely used methods to simulate quantum systems. A discretized path is constructed in the configuration space of the system subject to the appropriate boundary conditions. For example, closed paths or paths with one point fixed (say at the singularity in QC) could be chosen. Given a path, its discretized Euclidean action (2.10) can be computed. At this stage one could proceed by choosing paths at random in the configuration space and adding $\exp(-S_E)$ (for S_E the Euclidean action) to the PI. However, this is inefficient and computationally wasteful since most paths contribute little to the PI. Most schemes take advantage of some version of the Metropolis importance sampling algorithm [41] (MA) to preferentially select paths which contribute significantly to the PI. In its simplest version [13], one moves a single point on the original path to define a new path. The Euclidean actions of the two paths are compared. If the action of the new path is lower, the new path is kept. This drives the system to the least (Euclidean) action (i.e., lowest-energy) path. If the new path's action is the greater, but a call to a random number generator yields a (pseudo)random number in [0,1) less than $\exp(-S_{E,\rm new}+S_{E,\rm old})$, the new path is still kept to avoid trapping the simulation in a local minimum. Otherwise one reverts to the original path. The probability for acceptance of a move is controlled by the Euclidean time τ which acts as an inverse temperature and by the maximum stepsize in a move (usually chosen so that $\approx\frac{1}{2}$ the moves are accepted for a given τ). Eventually, the system relaxes to fluctuations about the classical (Euclidean) path. The algorithm selects paths

with the correct exponential weighting. If closed paths were used, any point on the path can be regarded to be its starting point. For both these reasons and Eq. (2.8) one obtains $|\psi_0(q)|^2$ as the distribution function of (moved) path points.

A variation of this method we have used is that due to Takehashi and Imada [14]. If there are M points on each path, the entire path is moved after M moves involving single points. The large move (MC step) is accented or rejected based on the MA. After each MC step, the distribution of path points is accumulated to eventually yield $|\psi_0(q)|^2$. This version of MA improves convergence. Several simulations are usually averaged to remove history dependence due to the MA, i.e., the paths are not strictly independent of each other since the simulation is a Markov process. Averaging independent simulations will remove unwanted correlations in sequential paths. The method is easily extended to many DF's at relatively little additional computation cost (particularly on a vector machine such as the Cray Y-MP).

MCPI simulations are sensitive to the "wrong sign" properties of the Hamiltonian constraint (2.1). In particular, the presence of a "hole" in the potential quickly causes the MA to drive the paths irrevocably into the hole. In order to obtain a well-defined simulation with this method, it is necessary to force the system to have a ground state either by inserting floors and walls as modifications of the potential or by driving essentially $|S_E|$ rather than S_E to a minimum. MCPI does not handle walls correctly if the potential is discontinuous. For example, the infinite square well does not yield the correct answer (the paths never relax since interior points do not "feel" the walls) although its approximation by a steep [e.g., $V(q) \propto q^6$] potential does. If the potential vanishes throughout some region, the system never relaxes there.

C. Semiclassical Monte Carlo (SCMC) path integral

This method, due to Wandzura [42], attempts to improve convergence by separately constructing the semiclassical (Euclidean) propagator which is then used as the basis for fluctuations generated by a MC simulation. Wandzura essentially bases his method on that of discrete PI (DPI) simulation. The DPI does not employ the MA. Instead, totally uncorrelated paths are generated point by point using a distribution of Gaussian random variables with adjustable mean and standard deviation chosen to reproduce the correct conditional probabilities. These are such that the Euclidean free particle measure

$$\exp\left[-\frac{1}{2}\int \dot{x}^2(t)dt\right] \tag{3.2}$$

is correctly generated when

$$\exp\left[-\int V[q(t)]dt\right]$$

is averaged over the set of paths. This method can converge very slowly since most paths will contribute little to the PI. Wandzura's scheme replaces the free particle measure with the semiclassical one including the semiclassical part of $\exp(-S_E)$. This will converge much faster if the semiclassical approximation is reasonably valid.

We find that with the semiclassical propagator [42]

$$\langle q,\tau|q',0\rangle_{\rm sc} = \left[-\frac{1}{2\pi}\frac{\partial^2 S_E}{\partial q\,\partial q'}\right]^{1/2} \exp(-S_E)\,, \tag{3.3}$$

the full propagator becomes

$$\langle q,\tau|q',0\rangle = \langle q,\tau|q',0\rangle_{\rm sc}\left\langle \exp\left[-\int_0^\tau [V[q_c(t)+y]-V_c(t)-yV_c'(t)-\tfrac{1}{2}y^2V_c''(t)]dt\right]\right\rangle\,, \tag{3.4}$$

where the subscript sc refers to evaluation at the classical Euclidean path and y is the fluctuating variable. Wandzura uses a generalization of DPI for the averaging denoted by angular brackets. The generalization to many DF's is given in Ref. [42] and represents non-negligible additional effort. There are several problems with this scheme particularly for more than one DF. The primary problem is that the classical Euclidean path is required for the simulation. This path is unique for fixed τ and $V(q)$ strictly a potential well since the Euclidean classical problem becomes a single scattering off a barrier. This scattering problem is numerically unstable for many DF's. (For convenience, the discussion will be in terms of closed paths.) The slightest error will cause the path to head off in the wrong direction rather than to double back on itself. Even shooting to the classical turning point is not consistently accurate for steep potentials such as that for the mixmaster cosmology. An approach that does appear to work starts from an arbitrary point *defined* to be the classical turning point and then integrates outward for the required τ. This procedure appears to be stable. Care is required, however, to generate path end points that are more or less uniformly distributed through configuration space. Recall that the desired wave function is to be evaluated at these path end points since they are really the initial points for the paths.

However, the need to use the classical path means that the simulation about it must be associated with a particular value of q—viz., the classical path's start and/or end point. This makes the SCMC method much less efficient than the MCPI (or MCD) since one can only find the wave function at a single point from each simulation. This becomes a very serious problem as the dimension of the configuration space increases. The computational effort for many DF's increases unreasonably since the array of simulations is not easily vectorizable. On the other hand, the totally independent simulations are ideally suited to massively parallel processing.

The possible advantage to QC simulations for the SCMC method is related to the fact that most of the "wrong sign" behavior can be traced to the DF associated with the volume expansion. In principle, $\langle q,\tau|q',0\rangle_{sc}$ could be found separately "by hand" and defined to include the "wrong sign" DF's. It is to be noted that semiclassical analysis to obtain the wave function has been performed on models as sophisticated as scalar field coupled to mixmaster [10]. It is to be hoped that this "factorization" of the bad behavior can leave a well-defined simulation in the residual DF's. It is also possible to modify Wandzura's version of the SCMC method to incorporate MA. This makes less use of the classical path, but is much easier to implement and appears to be more stable numerically.

IV. THE DE SITTER EXAMPLE

Perhaps the simplest cosmological model is the closed empty FRW universe with cosmological constant described by the Hamiltonian constraint [8]

$$H=p_a^2+\kappa a^2-\lambda a^4 , \tag{4.1}$$

where a is the cosmological scale factor and p_a its conjugate momentum. To obtain this form,the lapse has been chosen to yield Einstein's equations in conformal rather than comoving proper time. The potential terms in (4.1) are displayed in Fig. 1(a) for $\kappa=1$ and $\lambda=0.06$. [The mixmaster equipotentials shown in Fig. 1(b) will be discussed in the next section.] Note that in contrast with (2.3), H has been multiplied by an overall factor of -1. Although the potential $V(a)\rightarrow-\infty$ for large a, the small value of λ allows the system to behave as if it had a true ground state. Equivalently, the barrier is sufficiently high that for the unobserved Euclidean coordinate time τ large enough (in the simulations) the tunneling probability becomes extremely small.

To compare the methods discussed in Sec. III, a series of simulations was performed designed to be as similar as possible for the different methods. For convenience, the boundary condition imposed is that all paths be closed in a (i.e., $a_N=a_1$ for all paths). The results are shown in Fig. 2. The de Sitter model with $\kappa=1$ and $\lambda=0.06$ was used in all cases. To obtain some idea of accuracy (or at least reproducibility), four simulations of each type that differed only in the initial seed for the random number generator were averaged. The error bars display the dispersion among the independent simulations. (The correlations of MA and within MCD prevent internal computations of errors. The DPI and SCMC methods are uncorrelated but the internal error is misleadingly large, determined by the negligible contribution paths.) The simulations represent roughly the same computational effort.

From Fig. 2, the SCMC method appears to yield the most accurate wave function with MCPI a close second. We should note, however, that (4.1) with small λ is very close to the harmonic-oscillator Hamiltonian for which the semiclassical propagator is exact. The main conclusion to be drawn from this example is that all methods used elsewhere in physics to yield ground-state wave functions can also produce them for those QC models which have (effective) ground states.

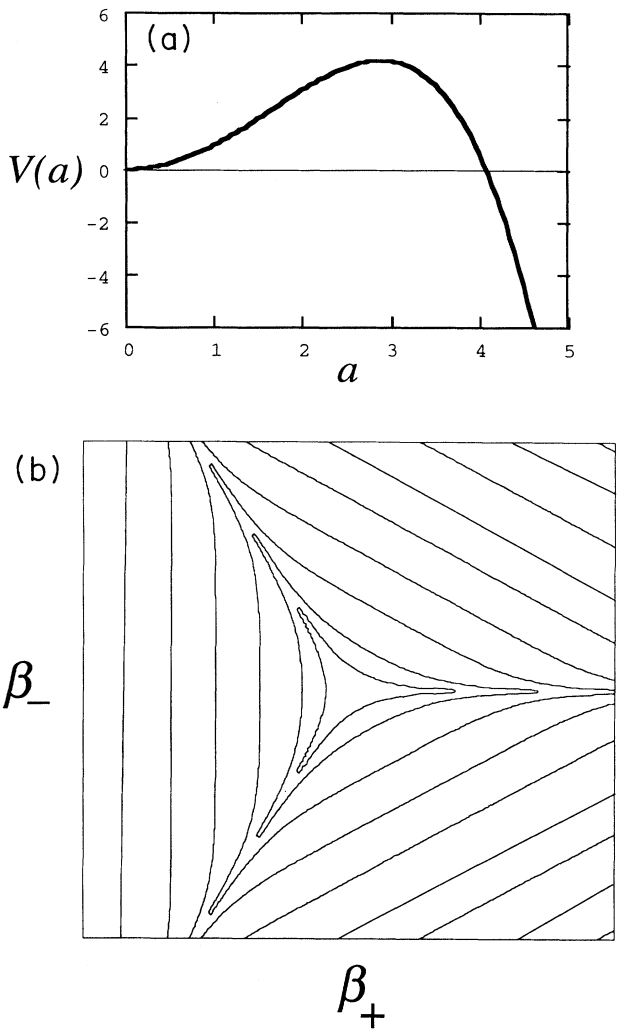

FIG. 1. Potential functions for Secs. IV and V. (a) $V(a)$ for the de Sitter model from Eq. (4.1) with $\lambda=0.06$ and $\kappa=1$. (b) Anisotropy plane equipotentials for the Bianchi-type IX potential given by Eq. (5.1).

For large values of λ, the tunneling probability becomes large (actually larger than the true tunneling probability since the original path configuration is not, in general, relaxed) and the system quickly leaks out. This will be discussed in some detail in Sec. VI.

V. THE MIXMASTER EXAMPLE

The mixmaster model is described by the Hamiltonian constraint (2.3) with

$$V(\beta_+,\beta_-)=e^{-8\beta_+}+2e^{4\beta_+}[\cosh(4\sqrt{3}\beta_-)-1] -4e^{-2\beta_+}\cosh(2\sqrt{3}\beta_-) . \tag{5.1}$$

Equipotentials of V are shown in Fig. 1(b). Recently, Kodama [43], Ryan and Moncrief [44], and Graham [45] have independently found a single exact quantum state

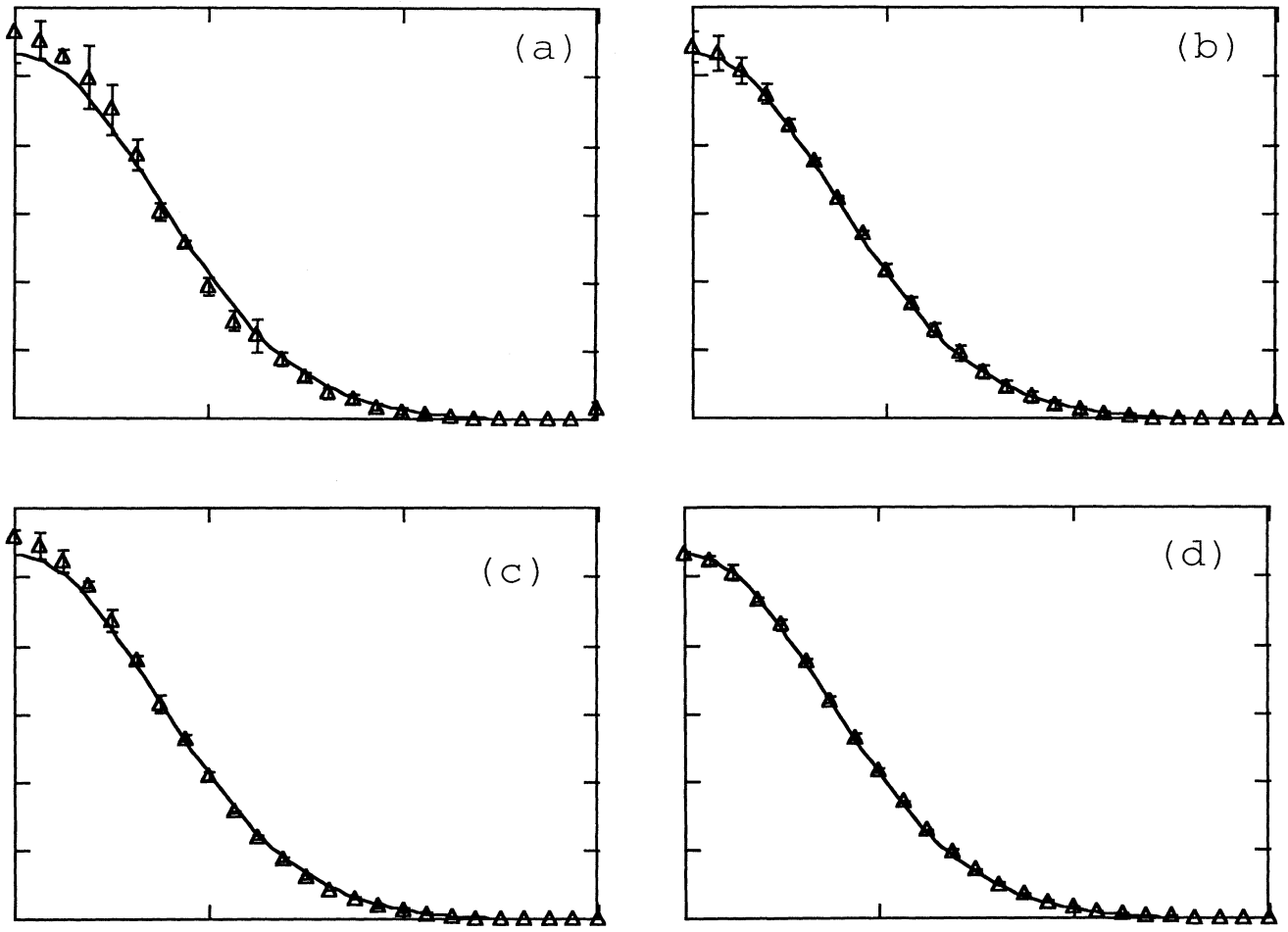

FIG. 2. A comparison of MC methods for the de Sitter model $H=p_a^2+a^2-0.06a^4$. In all cases, the horizontal axis is $0\leq a\leq 3$ and the vertical $0\leq|\Psi_0|^2\leq 1.2$. The triangles are from the simulation and the solid line using the shooting method to solve Schrödinger's equation for the given H. (a) MCD; (b) MCPI; (c) DPI; (d) SCMC method. In each case, error bars are generated from the standard deviation for each simulation point with four simulations that differ only in the initial seed of the random number generator.

for this system. A particular factor ordering is required. However, the characteristics of the state are reasonable and consistent with what would be expected on the basis of the classical solution. Their wave functions fill the triangular potential well uniformly near the singularity and peak at isotropy ($\beta_\pm=0$) for large Ω. (Semiclassical analyses, computer solutions, and numerical simulations also exist [10,21,46].)

The simulations to be described here are not well defined as given so that some *Ansatz* must be imposed to obtain any result. For the MCD method, it is necessary to perform a conformal rotation [$-p_\Omega^2\rightarrow+p_\Omega^2$ in H from (2.3)] and to take $|V(\Omega,\beta_+,\beta_-)|$. For the MCPI method, there are several options. (1) The MA can be modified so that $|S_E|\rightarrow 0$ rather than S_E. This should yield a ground state in which $\langle H\rangle=0$. No conformal rotation is required so that the correct sign relationship among all the terms in H is preserved. (2) Each segment in the skeletonized action (2.10) is replaced by its absolute value, i.e., if $S_E=\sum_k S_{E,k}$ use $|S_{E,k}|$ in the MA. (3) Place a floor under the action, e.g., require $S_{E,k}\geq 0$. The same simulation was performed using the three separate *Ansätze*. The results for a single ($\Omega\approx -3$) anisotropy plane wave-function cross section are shown in Fig. 3. The wave functions are qualitatively similar although the visible differences are real. *Ansatz* (1) is perhaps the most realistic and was used in [20,21]. In all cases, we shall assume the MSS paths to be closed.

The MSS wave functions for simulations of comparable computational effort are shown in Fig. 4. The MCD simulation in Fig. 4(a) shows rough qualitative agreement with the known exact solutions. The MCPI wave function shown in Fig. 4(b) "breaks up" at large Ω with significant probability for large anisotropy. Figure 4(c) shows the expectation values of $\beta_\pm$ using the simulation wave function. Near the singularity ($\Omega\rightarrow-\infty$), the

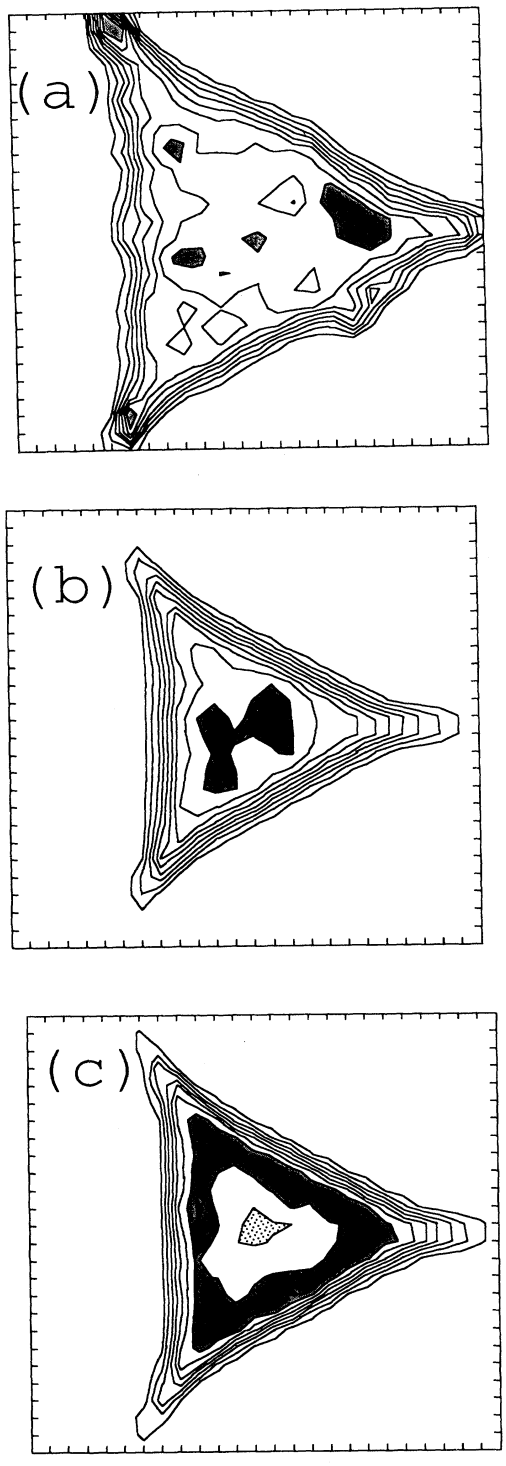

FIG. 3. A comparison of algorithms to bound S_E from below. An anisotropy plane slice of the absolute value squared of the wave function of the Bianchi-type IX model is shown for (a) $|S_E| \to 0$, (b) $|S_{E,k}| \to 0$, where $S_{E,k}$ is that part of the action associated with the kth segment of the discretized MSS path, and (c) $S_E > 0$ enforced by placing a floor below the action. The dark shading represents maxima and the light shading minima of the wave function.

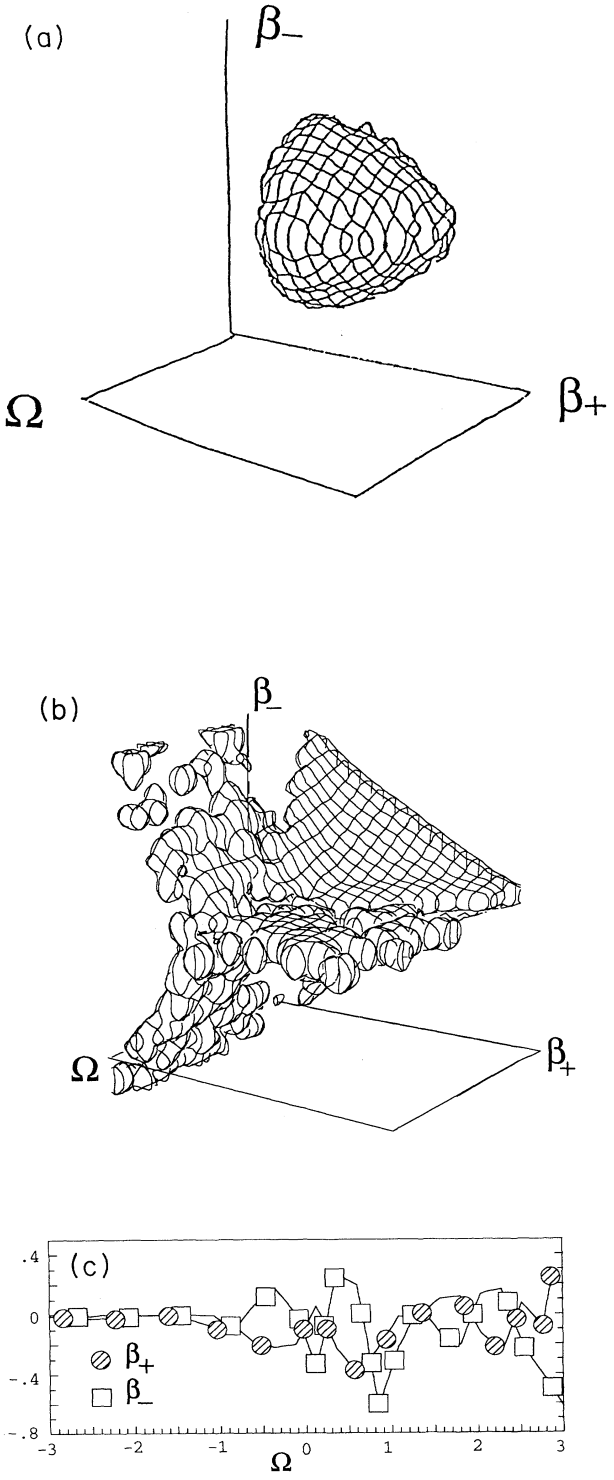

FIG. 4. Comparison of MCD and MCPI mixmaster simulations. (a) The region of the (Ω,β_+,β_-) MSS where $|\Psi_0|^2$ exceeds 0.01 for a MCD simulation using 40 000 *psips* and 1000 time steps. (Ω is increasing out of the paper.) (b) The same plot for a MCPI mixmaster study averaging ten independent simulations. (c) The expectation values of the anisotropy variables $\beta_\pm$ vs Ω. The *Ansatz* of Fig. 3(b) is used.

wave function is symmetric. At large Ω we should still have $\langle \beta_{\pm} \rangle = 0$ since the potential is still symmetric about the origin. This has been discussed elsewhere [21]. The differences between the two simulations can easily be understood in terms of the two simulation algorithms. The MSS equipotential for large Ω has narrow $V \leq 0$ channels with steep walls. The MCD algorithm will destroy any *psip* that wanders into a channel since almost any move in its random walk will bring it under the steep walls. Conversely, the MCPI algorithm causes the path points to get stuck in the channel. Almost all moves will bring the point under the steep walls greatly increasing the action so that the move will be rejected. It is not possible to choose between the methods without additional information.

An alternative version of the comparison between the MCD and MCPI methods is shown in Fig. 5. The MCD wave function is shown in Fig. 5(a). The simulation in Fig. 5(b) is the MCPI method designed to be as similar as possible to the MCD method. It includes the conformal rotation and the absolute value of the MSS potential required by the MCD method and starts the simulation with all path points at zero anisotropy. The resultant wave function is qualitatively similar to the MCD one. A more realistic (no conformal rotation, $|S_E| \rightarrow 0$ rather than $|V|$) simulation with initial path points at zero anisotropy is more like Fig. 5(a) than 4(b) in appearance.

We also consider simulations for the MCPI, DPI, and MCD methods made as close as possible to each other. The same cross section of the MSS wave function is compared in Fig. 6. There are clear qualitative differences.

The numerical difficulty of obtaining the classical paths for the SCMC method is particularly severe for the mixmaster model. Even a slight deviation from the harmonic oscillator—e.g., the model (4.1) regarded to be a spherical potential (but simulated in three-dimensional Cartesian coordinates) for $\kappa = 0.5$, $\lambda = 0.06$ required extensive effort. Shooting to the classical turning point [47] eventually proved sufficiently accurate (with Cray double precision and Bülirsch-Stöer integration [48]). The results are shown in Fig. 7. A simplified version of the SCMC method using MA rather than Wandzura's generalized DPI [42] was used.

Direct application of this simulation computer code to mixmaster failed. The classical paths could not be stably generated. It was therefore decided to select points at random near the MSS origin evolving them outward for Euclidean time τ regarding the starting point to be the classical turning point. The points at which the wave function could be evaluated became uncontrollable—they were wherever the trajectory might end. The distribution of path end points thus obtained is shown in Fig. 8(a). To increase the number of end points and enforce wave-function symmetry, the data set was replicated after 120° and 240° rotations. The pattern of points reflects the shape of the MSS potential (acting as a barrier for the Euclidean path). The (initial) classical turning points will have to be carefully adjusted to cover the entire region of the anisotropy plane (as desired). In the region with no end points in Fig. 8(a), the barrier falls away exponentially. The outward moving classical paths have approxi-

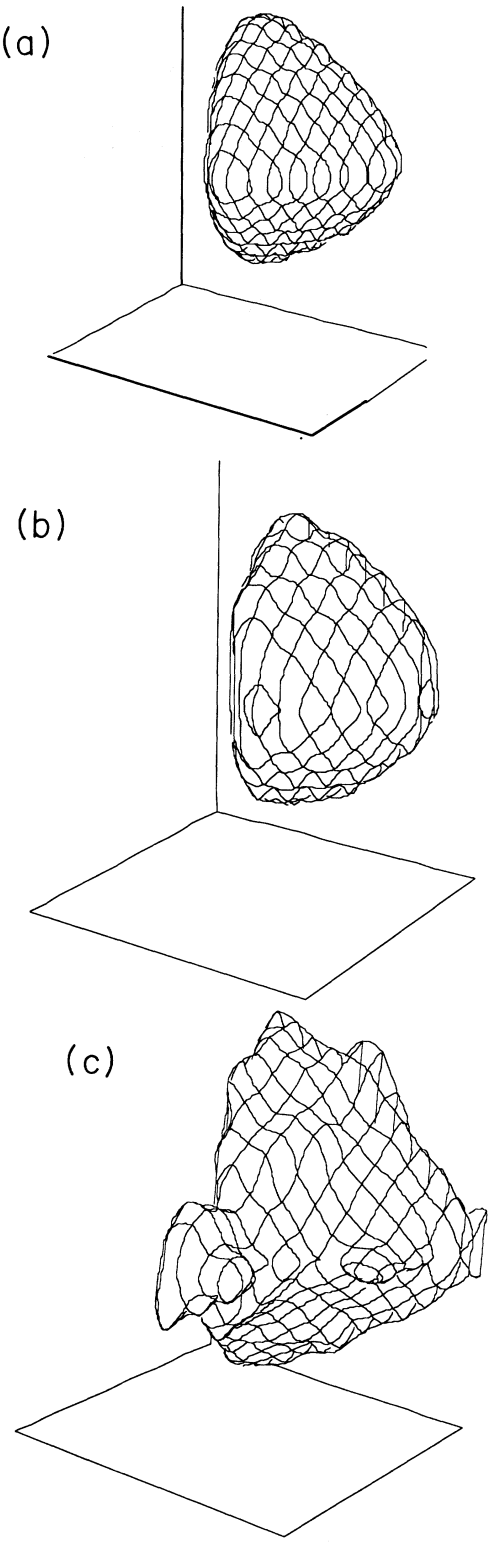

FIG. 5. Comparison of the MCD and MCPI with paths starting from zero anisotropy. (a) MCD for Bianchi-type IX vacuum; (b) MCPI with paths starting at $\Omega = -3$, $\beta_{\pm} = 0$, conformal rotation and the absolute value of $V(\beta_+, \beta_-)$; (c) MCPI with paths starting at $\Omega = -3$, $\beta_{\pm} = 0$, no conformal rotation, and the *Ansatz* of Fig. 3(a). In all cases, $\tau = 10$.

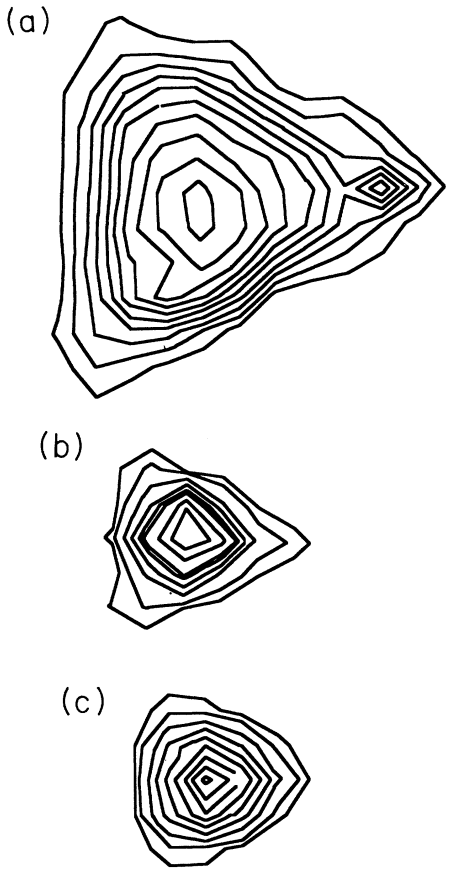

FIG. 6. The same MSS wave-function cross section for three simulation methods. (a) MCPI, (b) DPI, and (c) MCD.

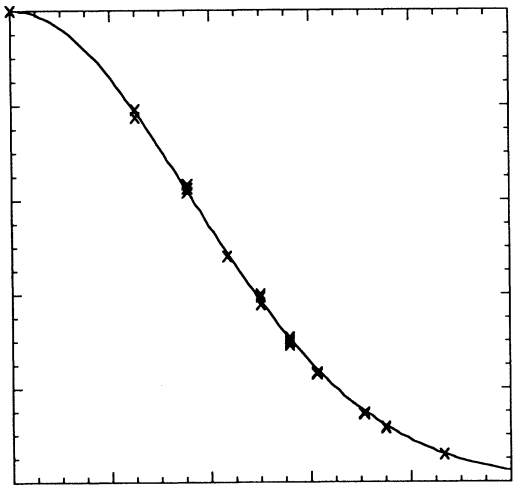

FIG. 7. The "spherical de Sitter" model test case for the SCMC method. The potential of Fig. 1(a) with $\kappa=0.5$, $\lambda=0.06$ is interpreted as a spherical potential with $0\le a\le 2$ a radial coordinate. A three-dimensional Cartesian coordinate SCMC simulation is performed. The horizontal axis is a and the vertical $0\le|\Psi_0|^2\le 1$. The crosses denote simulation values projected onto the radial direction. The solid line is the exact solution. A $5\times5\times5$ grid of initial path points was used.

mately zero energy (and thus begin near the top of the barrier). Thus they tend either to end before reaching this region or to overshoot it in the fixed available time τ. The Ω values are correlated with the anisotropy plane values as shown in Fig. 8(b). The large Ω (contour peaks) end points lie preferentially in the corners of the potential while low Ω values prefer the region near isotropy. At large Ω, the steepness of the potential is emphasized so that only the corners with $V\approx 0$ are accessible.

The classical path associated with each end point was used to compute the wave function at that end point. The results were binned with each bin normalized by the number of end points falling within it. This yielded correct relative values of $|\Psi_0|^2$ in the region of MSS

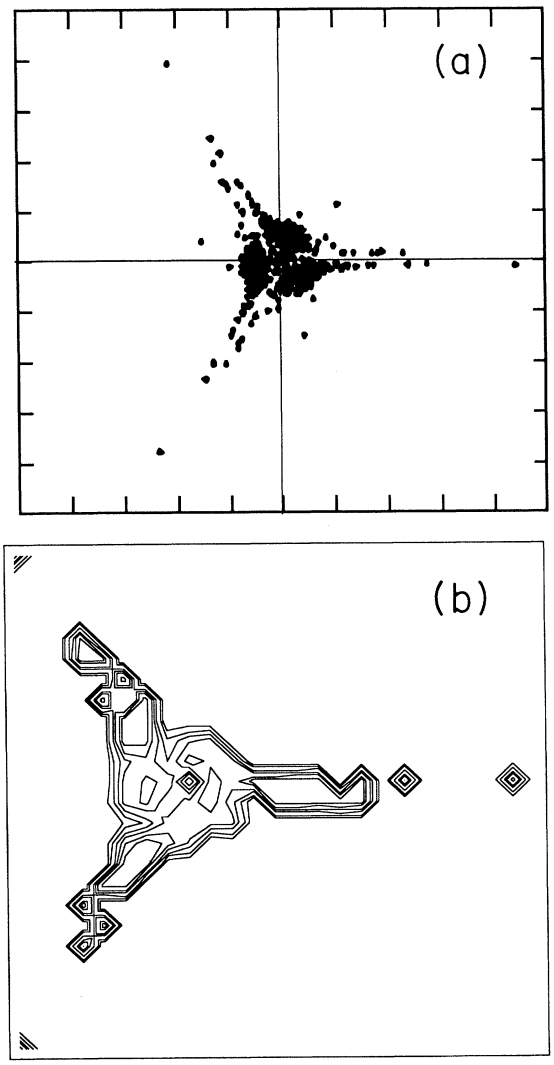

FIG. 8. Distribution of path end points. The horizontal axis is β_+ and the vertical β_- with $|\beta_\pm|\le 2.5$. (a) The data set for the anisotropy plane projection has been replicated to enforce 120° symmetry. Paths were started (randomly) near the origin with zero velocity (classical turning point boundary conditions) and evolved outward for fixed Euclidean time. (b) Distribution of Ω values are indicated by contours in the anisotropy plane with larger Ω as the peaks of the contour plot for the same data as (a).

where end points existed. Unfortunately, there were sufficiently few points that only three bins in Ω were used. The wave function for the three bins in Ω is shown in Fig. 9. The shape evidently reflects the distribution of path end points with Ω. This SCMC procedure is computationally wasteful on a vector machine. Future progress awaits its removal to a massively parallel processing computer.

VI. OTHER STUDIES

Here we shall consider a variety of analyses using primarily the MCPI method.

A. The validity of the MSS approximation

Since it is easy to add DF's to the MCPI method, one can test the validity of the MSS "approximation" (within the *Ansätze* required to obtain a well-defined problem) by comparing the wave function for an N DF problem to the N-dimensional projection of an $M+N$ DF problem (that classically contains the smaller problem). This has been discussed elsewhere [23]. The analysis is in the spirit of that of Kuchař and Ryan [7] since we consider a "micro-superspace" subspace of MSS. Here we shall present only one example—the addition of a scalar field to the mixmaster model. The Hamiltonian constraint for this model is

$$2H=-p_\Omega^2+p_+^2+p_-^2+p_\phi^2+e^{4\Omega}V(\beta_+,\beta_-) +e^{6\Omega}[\Lambda+\lambda(\phi^2-\mu^2)^2]\,, \tag{6.1}$$

where V is given by (5.1). Here Λ is a true cosmological constant and λ is the coupling constant for the self-interacting scalar field with "mass" parameter μ^2. The form chosen for the scalar field is one commonly used in inflationary models. It is clear that the scalar field couples as an effective cosmological constant to the background spacetime. If the ϕ DF is removed, the vacuum mixmaster model (with or without Λ) is regained. If the $\beta_\pm$ DF's are removed, the model becomes RWϕ (scalar field in a FRW universe). Several cases are considered with the boundary condition that the MSS paths be closed. The projection of the wave function into the subspace of interest is performed by computing the path point distribution (in the MCPI method) only binning in the variables associated with the subspace of interest without regard to the values of the remaining DF's for each path point. Results are shown in Fig. 10. For completeness, Fig. 10(a) shows the RWϕ potential. Figures 10(b) and 10(c) show the projected mixmaster+scalar field and RWϕ wave functions, respectively, in the Ω-ϕ plane. [The models use $\Lambda=0$, $\lambda=\mu=1$, and, for the RWϕ model, the constant curvature term that survives in (6.1) when $\beta_\pm=0$.] The wave functions are qualitatively quite similar. This is not too surprising since the scalar field and anisotropy DF's couple only through the volume DF. Figure 10(d) shows the MSS wave function for the vacuum mixmaster model. In Fig. 10(e), we see the (Ω,β_+,β_-) MSS projection of the same mixmaster+scalar field model shown in Fig. 10(b). Figure 10(f) is again a vacuum mixmaster model but with $\Lambda>0$ to illustrate differences between a true cosmological constant and the effective one due to the scalar field. Again the wave functions are similar particularly at small values of Ω. The possibly spurious "breakup" regions at large Ω are model dependent [21]. This is due to the fact that the breakup does not appear if the paths cannot reach large Ω. The $e^{6\Omega}$ dependence of the cosmological constant and scalar field terms greatly increases the action for path points at large Ω (unless $\phi^2\approx\mu^2$) confining the paths primarily to small Ω values if these terms are present.

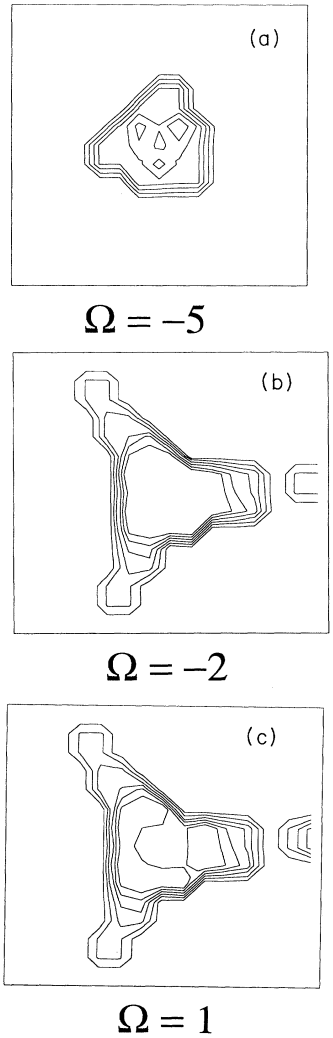

FIG. 9. Constant Ω cross sections of the SCMC mixmaster wave function $|\Psi_0|^2$. The paths attached to the end points shown in Fig. 8 are used individually to compute the wave-function value for that path. The results are binned with a weighting to remove the uneven end-point distribution. The wave function is set to zero in the regions of MSS where no path end point resulted.

B. Two studies involving the choice of time coordinate

In Fig. 10(d), the MCPI vacuum mixmaster model is run assuming the 3 DF's Ω, $\beta_\pm$ to be on an equal footing.

In Fig. 11 the same model is run assuming restrictions on the volume DF Ω. Such restrictions implicitly regard Ω to play the role of a time variable and have been used by others [47]. Figure 11(a) shows the wave function that results when the jth point on the MSS path is required to have the fixed value Ω_j (where the Ω values are distributed linearly in the range $|\Omega| \leq 3$). Thus the simulation reverts (in effect) to one with 2 DF's. Since large Ω values must occur on all paths, the wave-function "breakup" is emphasized. In Fig. 11(b), the Ω values are required to be ordered along each path. (The path points are already ordered in coordinate time τ.) We have continued to require the paths to be closed in Ω so that the maximum Ω value is required to occur on the midpoint of the path. Otherwise the Ω values are arbitrary. Here the wave function follows the narrowing of the channels at large Ω without breaking up and otherwise follows the potential shape until is abruptly cuts off.

We have also attempted to implement the time variable proposal of Unruh and Wald [25] for the RWϕ model. Essentially, they suggest that one can make the WD equation (2.2) a true Schrödinger equation by replacing the zero on the right-hand side with $\Lambda\Psi$. The arbitrary cosmological constant Λ appears formally as an energy eigenvalue. They construct (at least in MSS) states of the system as eigenstates of Λ. This can be interpreted in two ways. One can consider the original $\Lambda=0$ simulation to be an attempt to find the "zero-energy" eigenstate of the energylike Λ. Alternatively, the variable Λ can be added to the configuration space. We implement the latter al-

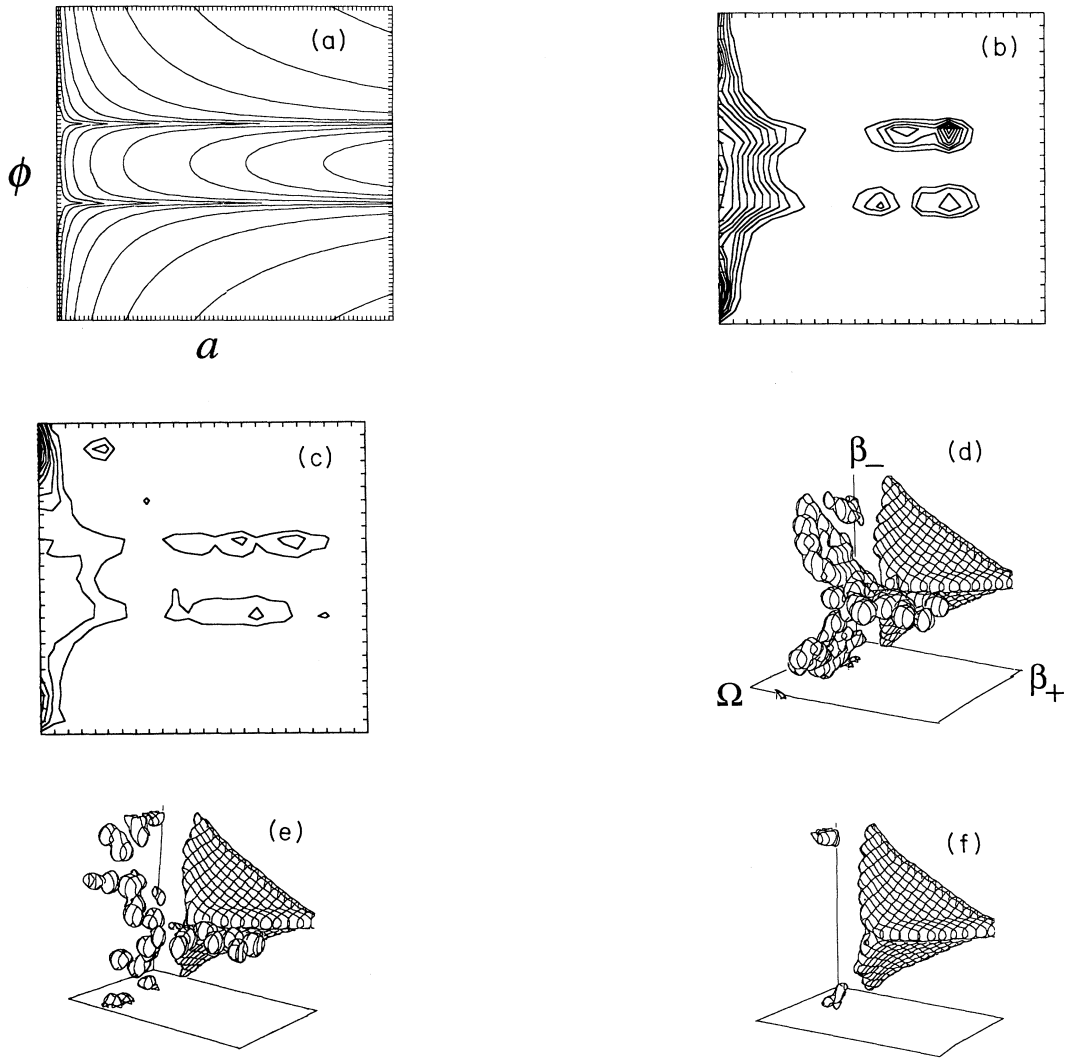

FIG. 10. Various projections of the mixmaster+scalar field model vs mixmaster and RWϕ wave functions. The models are all described by the constraint (6.1). (a) The potential for the RWϕ model in the a-ϕ plane where $a=\ln\Omega$. (b) The Ω-ϕ projection of the mixmaster+scalar field wave function. (c) The $\Omega-\phi$ RWϕ wave function. (d) The vacuum mixmaster wave function in the (Ω,β_+,β_-) MSS. (e) The (Ω,β_+,β_-) projection of the mixmaster+scalar field wave function. (f) The (Ω,β_+,β_-) wave function for mixmaster with positive cosmological constant.

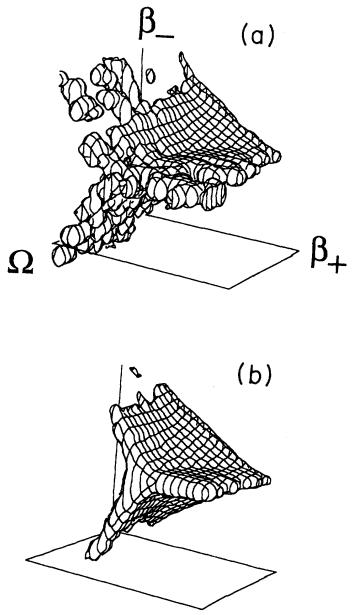

FIG. 11. Restrictions on Ω values in the mixmaster MCPI simulations. The parameters for the simulation are the same as those in Fig. 10(d). (a) The MSS wave function for a fixed value of Ω associated with each path point. The values are ordered and linear in the range $-3 \leq \Omega \leq 3$. (b) The MSS wave function for ordered but otherwise unrestricted Ω values. The ordering begins from a minimum Ω value to a maximum at the path midpoint and back to close the path in Ω.

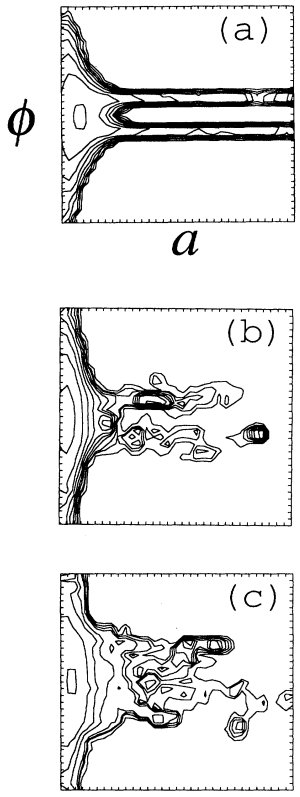

FIG. 12. Time choice in the RWφ model with cosmological constant Λ. (a) The wave function for a self-interacting minimally coupled scalar field is shown in the (a,ϕ) MSS where a is the scale factor and ϕ the scalar field amplitude for $\Lambda=0$. (b) The same model is shown for Λ determined by the simulation but restricted to be non-negative. (c) The same model for arbitrary Λ determined by the simulation.

ternative in the RWφ simulation [see Fig. 10(a)], by adding a variable cosmological constant to the action for the model [Eq. (6.1) with the $\beta_{\pm}$ DF zeroed out]. The wave function with $\Lambda=0$ (the first interpretation) is shown in Fig. 12(a). Figures 12(b) and 12(c) show the wave function obtained with variable Λ restricted to be non-negative and completely arbitrary respectively.

C. The ADM reduction

In a related manner we perform the ADM reduction by changing the weighting function in the MCPI method [28]. We consider the conformal scalar field added to the de Sitter model of Sec. IV. The Hamiltonian constraint (in conformal coordinate time) is [8]

$$H=-p_a^2+p_\chi^2-\kappa a^2+\Lambda a^4+\chi^2 \ . \tag{6.2}$$

Note that we have reverted to the original signs in H. The path integral (2.4) can implement the ADM reduction with the measure

$$\mathcal{D}[p_a,p_\chi,a,\chi]=\lim_{n\to\infty}(2\pi)^{-2n}\prod_{k=1}^{n}dp_{\chi,k}dp_{a,k}da^k d\chi^k d\alpha^k |p_{a,k}|\delta(a^k-a^i-k\Delta)\delta(a^n-a^f)\delta(\chi^n-\chi^f) \tag{6.3}$$

for the action

$$S=\sum_{k=1}^{n}\left[p_{\chi,k}(\chi^k-\chi^{k-1})+p_{a,k}(a^k-a^{k-1})-\frac{\alpha^k}{2}(-p_a^2+p_\chi^2-\kappa a^2+\lambda a^4+\chi^2)\right] , \tag{6.4}$$

where a is the scale factor, χ is conformally related to the scalar field amplitude, i and f refer to initial and final values, and the absolute value in (2.13a) is the quantum-mechanical relic of the Faddeev-Popov determinant. The first δ function in the measure is the gauge condition for Δ, a fixed interval of the scale factor a chosen to be the intrinsic time coordinate. The propagator can be exactly evaluated to yield, for a chosen to be the intrinsic time coordinate and χ the remaining dynamical DF associated with the conformal scalar field and closed paths,

$$\langle \chi, a_0 | \chi, a_f \rangle = \sum_{N=0}^{\infty} \varphi_N^2(\chi) \exp\left[- \int_{a_0}^{a_f} da \, | \Lambda a^4 - \kappa a^2 + 2N + 1 |^{1/2} \right] . \tag{6.5}$$

The absolute value in the intergrand is required for convergence. An equivalent form for this propagator is [see (2.13) for $N=2$ DF's]

$$\langle \chi, a_0 | \chi, a_f \rangle = \prod_{\text{paths}} \frac{V^{1/2}(\chi, a)}{\Delta s} K_1(V^{1/2} \Delta s) , \tag{6.6}$$

where

$$V = | \Lambda a^4 - \kappa a^2 + \chi^2 | \tag{6.7}$$

and

$$\Delta s = | -(\Delta a)^2 + (\Delta \chi)^2 |^{1/2} . \tag{6.8}$$

The absolute values are required to ensure that (6.6) is real since K_1 is a modified Bessel function. In the simulations, the weight function e^{-S_E} in MCPI is replaced by that on the right-hand side of (6.6). The exact solution is computed directly from (6.5) (including the first few modes). The results are shown in Fig. 13 for $\kappa = \pm 1$.

D. Tunneling in a modified de Sitter-like potential

Finally, we consider tunneling [48] in a modified de Sitter-like potential [shown in Fig. 14(a)] given by [49]

$$V(a) = \left[1 - 2 \exp\left[-\frac{1}{2b} \right] \right] \frac{1}{a} \exp\left[\frac{1 - a^2}{2} \right] + 2 \exp\left[-\frac{(a-2)^2}{2b} \right] - 1 \tag{6.9}$$

for $b = 0.297\,85$. This is smoother than the de Sitter potential, but has the same features. Figure 14(a) shows the wave function for an MCPI simulation evaluated after increasing numbers of MC steps. The shape of the wave function changes from an initial confinement in the well portion of the potential to one with significant probability to be at large a. A series of 100 simulations was run for up to 22 500 MC steps. Of these, 33 never tunneled. A simulation was defined to have tunneled if the expectation value of a reached the value of a at which $V(a)$ becomes negative. Figure 14(b) displays $\langle a \rangle$ versus the MC step number N for two simulations, one of which tunneled and other did not. The differences are apparent very early in the simulation. The simulations that did in fact tunnel did so at different values of N. A histogram of the number of simulations tunneling at a given N vs N is shown in Fig. 14(c) (with triangles). For comparison, a similar study with MCD simulations was plotted on the same graph (with diamonds). Early in the simulation, the two methods yield very different results. MCPI simulations show approximately constant tunneling likelihood while MCD shows a steep rise. Both then show very similar exponential decays in the tunneling likelihood. We must emphasize here that both the horizontal and vertical axes have been adjusted for the two simulations to match the peaks. We must also not forget that N has nothing to do with time in the MCPI although it measures Euclidean time in MCD. The exponential tails in Fig. 14(c) are suggestive of a decaying metastable state [50].

VII. DISCUSSION

Well-known quantum MC simulation methods have been applied to QC. Each of the methods considered—MCD, MCPI, and SCMC simulations—can yield the correct wave function for systems such as the de Sitter

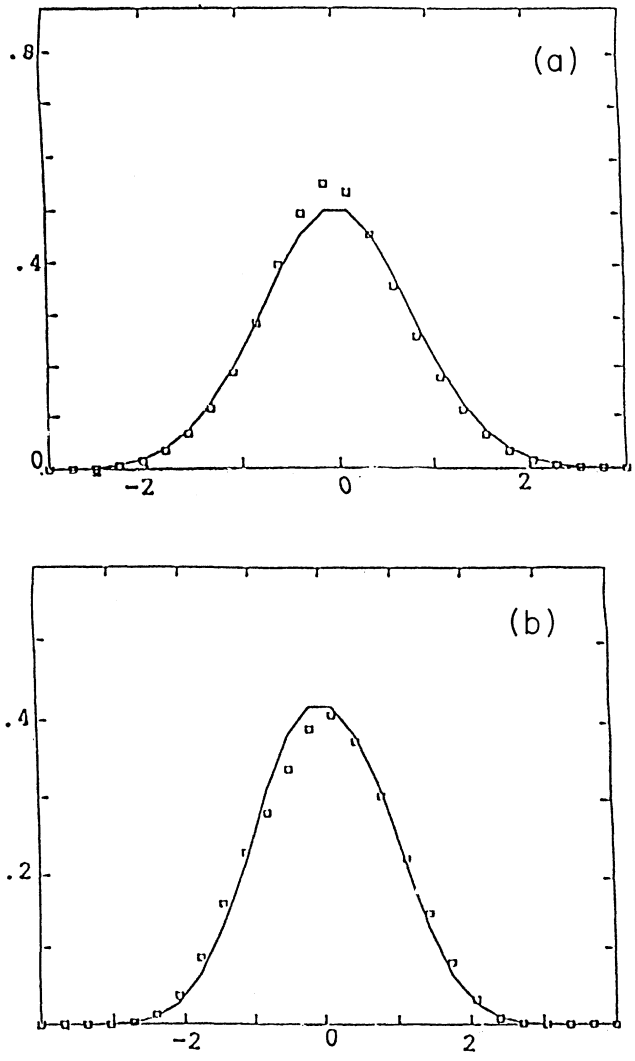

FIG. 13. ADM reduction in MCPI: $|\Psi_0|^2$ vs χ. The model from (6.2) is evaluated using the Bessel function weighting of (6.6) to generate the open squares. The solid line is the solution obtained by evaluation of (6.5). (a) $\kappa = -1$, $a_0 = 0.1$, $a_f = 8.0$, $\Lambda = 0.01$. (b) $\kappa = +1$, $a_0 = 1.0$, $a_f = 10.0$, $\Lambda = 0.1$.

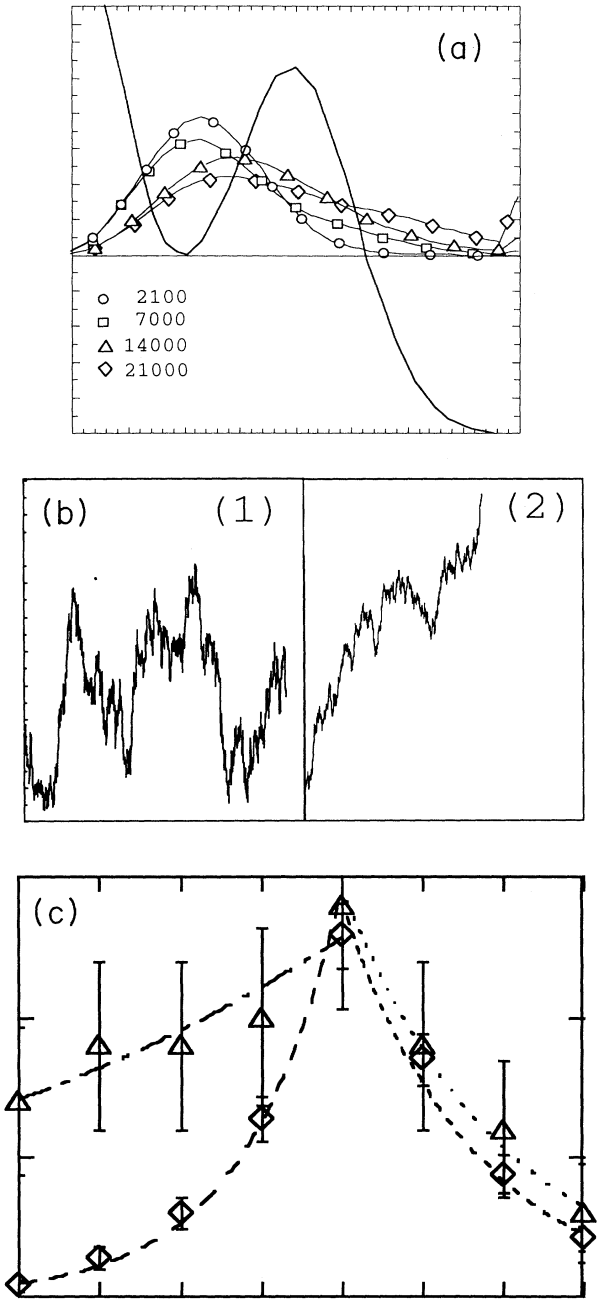

FIG. 14. Tunneling in the modified de Sitter potential. (a) The simple solid line is $V(a)$ from (6.9) vs a with $0 \leq a \leq 4$ (and V on its own scale). The remaining curves are $|\Psi_0|^2$ vs a for different numbers of MC steps (as indicated). (b) $\langle a \rangle$ computed during the simulation vs MC step number for a simulation that never tunnels (1) and one that does (2). The wave function is assumed to tunnel if $\langle a \rangle > 2.640\,817$, the value at which $V(a)$ becomes negative. (c) Histogram of the number of simulations, $\mathcal{N}$, which tunnel at the Nth MC step or Nth $\Delta\tau$ step vs N for MCPI (triangles) or MCD (diamonds), respectively. The vertical and horizontal axis scales were adjusted to yield the best match at the peaks (with eight bins). The dotted lines to the right of the peak are best-fit exponentials. Error bars represent $\sqrt{\mathcal{N}}$ in all cases.

universe for small cosmological constant, which in effect have a ground state. On the other hand, the solution to the WD equation for this model [8,11,32] becomes oscillatory for large a for any boundary condition that keeps the overall sign for the Hamiltonian constraint in (4.1). This oscillatory behavior is physically consistent with an expanding universe that can reach arbitrarily large a. For the de Sitter model with large cosmological constant [or the qualitatively similar potential (6.7)], the path or *psip* distribution initially localized near the origin quickly tunnels out to large a. Unfortunately but not unphysically, the system never relaxes in the "free" region so that a wave function cannot be constructed. It is also not yet clear how correctly the tunneling in, e.g., Fig. 14 models the actual tunneling process.

For more complicated models, such as mixmaster and its generalizations, different MC methods yield qualitatively different results. Although these differences can be understood in terms of each method's algorithm, it is not clear on what basis one should decide which method to prefer. If the model is forced to have a ground state, various studies can be made. So far, we have considered the validity of the MSS approximation by ignoring M DF's of an $N+M$ DF system. The results of Fig. 10 appear to confirm the conclusions of Kuchař and Ryan [7] that the MSS approximation can be trusted if the neglected DF's do not interact significantly with those that are kept. We also have shown that it is easy to study various proposals for choice of time variable. Even the ADM reduction within the PI can be achieved with a change of path weighting function. Although the wave function itself has been of primary interest here, it requires little extra effort to generate expectation values of observables as their simulation averages.

Still, the problem of the Hamiltonian constraint's unboundedness from below remains a serious obstacle to the entire MC approach. It might be possible to use some version of Wandzura's SCMC method to isolate the volume DF primarily responsible for the bad behavior. So far, numerical difficulties have impeded progress in implementation of this approach. We are about to begin study of this method on the massively parallel Connection Machine. Other proposals to deal with "bottomless actions" [16–19] are currently under investigation. Finally, it should be mentioned that similar issues involving quantum MC simulations are being addressed at the more sophisticated level of quantum field theory of the nonlinear σ model (as a nonrenormalizable test case for quantum gravity) by DeWitt and co-workers [51].

ACKNOWLEDGMENTS

This work was supported in part by NSF Grant Nos. PHY-8904847 and PHY-9107162 to Oakland University. The author is grateful for hospitality provided by the Institute for Geophysics and Planetary Physics at Lawrence Livermore National Laboratory. Computations were performed with the facilities of the National Center for Supercomputing Applications at the University of Illinois.

[1] G. Smoot *et al.*, Astrophys. J. **396**, L1 (1992).
[2] M. Gell-Mann and J. B. Hartle, in *Complexity, Entropy, and the Physics of Information,* edited by W. H. Zurek (Addison-Wesley, Reading, 1990); B. L. Hu, in *Thermal Fields and Their Applications,* edited by H. Ezawa *et al.* (North-Holland, Amsterdam, 1991); W. H. Zurek, Phys. Rev. D **24**, 1516 (1981); **26**, 1862 (1982); Phys. Today **44**, 36 (1991); H. D. Zeh, Phys. Lett. A **116**, 9 (1986).
[3] For recent reviews see R. Laflamme, in *Quantum Gravity and Cosmology,* edited by J. Perez-Mercader and J. Sola (World Scientific, Singapore, 1992); B. K. Berger, in *Directions in General Relativity,* Vol. 1: Papers in Honor of Charles Misner, edited by B. L. Hu, M. P. Ryan, and C. V. Vishveshwara (Cambridge University Press, Cambridge, England, 1993); a comprehensive bibliography to 1990 can be found in J. J. Halliwell, Int. J. Mod. Phys. A **5**, 2473 (1990).
[4] See, for example, J. Guven and M. P. Ryan, Jr., Phys. Rev. D **45**, 3559 (1992); K. Kuchař, in *Proceedings of the 4th Canadian Conference on General Relativity and Relativistic Astrophysics,* edited by G. Kunstatter, D. Vincent, and J. Williams (World Scientific, Singapore, 1992).
[5] C. W. Misner, Phys. Rev. **186**, 1319 (1969); in *Magic without Magic,* edited by J. Klauder (Freeman, San Francisco, 1972), pp. 441–473.
[6] B. S. DeWitt, Phys. Rev. **160**, 1113 (1967).
[7] K. Kuchař and M. P. Ryan, in *Gravitational Collapse and Relativity,* edited by H. Sato and T. Nakamura (World Scientific, Singapore, 1986); Phys. Rev. D **40**, 3982 (1989).
[8] J. B. Hartle and S. W. Hawking, Phys. Rev. D **28**, 2960 (1983).
[9] S. W. Hawking, Nucl. Phys. **B239**, 257 (1984); J. J. Halliwell and J. Louko, Phys. Rev. D **39**, 2206 (1989).
[10] S. W. Hawking and J. C. Luttrell, Phys. Lett. **143B**, 83 (1984).
[11] A. Vilenkin, Phys. Rev. D **37**, 888 (1988); **39**, 1116 (1989).
[12] See, for example, S. E. Koonin, and D. C. Meredith, *Computational Physics (Fortran Version)* (Addison-Wesley, Redwood City, California, 1990), Chap. 8.
[13] S. V. Lawande, C. A. Jensen, and H. L. Sahlin, J. Comput. Phys. **3**, 416 (1969); **4**, 451 (1969).
[14] M. Takahashi and M. Imada, J. Phys. Soc. Jpn. **53**, 963 (1984); **53**, 3765 (1984).
[15] R. P. Feynman, Rev. Mod. Phys. **20**, 367 (1948); M. S. Marinov, Phys. Rep. **60**, 1 (1980).
[16] E. Meyers, Class. Quantum Grav. **9**, 405 (1992).
[17] M. Carreau, E. Farhi, S. Gutmann, and P. F. Mende, Ann. Phys. (N.Y.) **204**, 186 (1990).
[18] J. Greensite and M. B. Halpern, Nucl. Phys. **B242**, 167 (1984).
[19] J. D. Brown and E. A. Martinez, Phys. Rev. D **42**, 1931 (1990).
[20] B. K. Berger, Gen. Relativ. Gravit. **20**, 755 (1988).
[21] B. K. Berger, in *Fifth Marcel Grossmann Meeting,* Proceedings, Perth, Australia, 1988, edited by D. G. Blair and M. J. Buckingham (World Scientific, Singapore, 1989); Phys. Rev. D **39**, 2426 (1989).
[22] P. Kerr and B. K. Berger, in *Fifth Marcel Grossmann Meeting* [21].
[23] B. K. Berger, in *Sixth Marcel Grossmann Meeting on General Relativity,* Kyoto, Japan, 1991, edited by H. Sato (World Scientific, Singapore, 1992).
[24] R. Arnowitt, S. Deser, and C. W. Misner, in *Gravitation: An Introduction to Current Research,* edited by L. Witten (Wiley, New York, 1962), pp. 227–265.
[25] W. G. Unruh and R. M. Wald, Phys. Rev. D **40**, 2598 (1989).
[26] A. Vilenkin, Nucl. Phys. **B252**, 141 (1985); Phys. Rev. D **33**, 3560 (1986).
[27] M. P. Ryan, Jr. and L. C. Shepley, *Homogeneous Relativistic Cosmologies* (Princeton University, Princeton, 1975); M. MacCallum, in *General Relativity: An Einstein Centenary Survey,* edited by S. W. Hawking and W. Israel (Cambridge University Press, Cambridge, England, 1979).
[28] B. K. Berger and C. N. Vogeli, Phys. Rev. D **32**, 2477 (1985); B. K. Berger, *ibid.* **32**, 2485 (1985); in *Origin and Early History of the Universe,* edited by J. Demaret (Universite de Liège, Leïge, Belgium, 1987), pp. 45–52.
[29] A. Hosoya and M. Morikawa, Phys. Rev. D **39**, 1123 (1989); M. McGuigan, Phys. Rev. D **38**, 3013 (1988); A. Zhuk, "Integrable Multidimensional Quantum Cosmology," report (unpublished).
[30] J. B. Hartle, in *Relativistic Astrophysics,* Proceedings of the Thirteenth Texas Symposium, Chicago, Illinois, 1986, edited by M. P. Ulmer (World Scientific, Singapore, 1987), pp. 80–96; in *Proceedings of the 12th International Conference on General Relativity and Gravitation,* edited by N. Ashby, D. F. Bartlett, and W. Wyss (Cambridge University Press, Cambridge, England, 1990).
[31] A. O. Barvinskii and V. N. Ponomarev, Phys. Lett. **167B**, 289 (1986); H. D. Conradi, Phys. Rev. D **46**, 612 (1992); Y. Kazama and R. Nakayama, *ibid.* **32**, 2500 (1985); C. Kiefer, *ibid.* **38**, 1761 (1988); V.A. Rubakov, Phys. Lett. **148B**, 280 (1984); S. Wada, Phys. Rev. Lett. **59**, 2375 (1987); A. Zhuk, Class. Quantum Grav. **5**, 1357 (1988).
[32] W. M. Suen and K. Young, Phys. Rev. D **39**, 2201 (1989).
[33] See, for example, J. J. Halliwell, in *Proceedings of the Osgood Hill Meeting on Conceptual Problems in Quantum Gravity,* edited by A. Ashtekar and J. Stachel (Birkhauser, Boston, 1989).
[34] S. W. Hawking and D. N. Page, Nucl. Phys. **B264**, 185 (1986); K. Kuchař, Phys. Rev. D **34**, 3044 (1987); **35**, 596 (1987).
[35] C. Itzykson and J. B. Zuber, *Quantum Field Theory* (McGraw-Hill, New York, 1978), Chap. IX.
[36] J. B. Anderson, J. Chem. Phys. **63**, 1499 (1975).
[37] J. B. Hartle and K. V. Kuchař, J. Math. Phys. **25**, 57 (1984); Phys. Rev. D **34**, 2323 (1986).
[38] K. Schleich, Phys. Rev. D **39**, 2192 (1989); K. Schleich, Class. Quantum Grav. **7**, 1529 (1990); C. Teitelboim, Phys. Rev. Lett. **38**, 1106 (1977); Phys. Lett. **96B**, 77 (1980); Phys. Rev. D **25**, 3159 (1982); **28**, 297 (1983).
[39] P. L. Kerr, "A Monte Carlo Diffusion Approach to Quantum Cosmology," Master's thesis, Oakland University, 1988.
[40] See, for example, S. W. Hawking, in *General Relativity: An Einstein Centenary Survey* [27].
[41] N. Metropolis, A. W. Rosenbluth, M. N. Rosenbluth, A. H. Teller, and E. Teller, J. Chem. Phys. **21**, 1087 (1953).
[42] S. M. Wandzura, Phys. Rev. Lett. **57**, 2603 (1986).
[43] H. Kodama, Prog. Theor. Phys. **80**, 1024 (1988).
[44] M. P. Ryan, Jr. and V. Moncrief, Phys. Rev. D **44**, 2375 (1991).
[45] R. Graham, Phys. Rev. Lett. **67**, 1381 (1991).
[46] R. Graham and P. Szepfalusy, Phys. Rev. D **42**, 2483 (1990); T. Furusawa, Prog. Theor. Phys. **75**, 59 (1986); **76**, 67 (1986); W. A. Wright and I. G. Moss, Phys. Lett. **154B**, 115 (1985).

[47] See, for example, W. H. Press, B. P. Flannery, S. A. Teukolsky, and W. T. Vetterling, *Numerical Recipes: The Art of Scientific Computing* (Cambridge University Press, Cambridge, England, 1986).

[48] Similar computations in the de Sitter model can be found in R. Church, "Monte Carlo Simulations for a Tunneling Origin of the Universe," Master's thesis, Oakland University, 1990.

[49] M. McClendon and H. Rabitz, Phys. Rev. A **37**, 3479 (1988).

[50] G. Jona-Lasinio, F. Martinelli, and E. Scoppola, Lett. Nuovo Cimento **34**, 13 (1982).

[51] B. S. DeWitt, in *Geometrical and Algebraic Aspects of Nonlinear Field Theory,* Proceedings of the International Meeting, Amalfi, Italy, 1988, edited by S. De Filippo *et al.* (North-Holland, Amsterdam, 1989), pp. 97–112; B. S. DeWitt, E. Myers, R. Harrington, A. Kapulkin, J. de Lyra, S. K. Foong, and T. Galivan, in *Quantum Gravity,* Proceedings of the Fifth Seminar, Moscow, USSR, edited by M. A. Markov, V. A. Berezin, and V. P. Frolov (World Scientific, Singapore, 1991); J. de Lyra, B. DeWitt, S. K. Foong, T. Gallivan, R. Harrington, A. Kapulkin, E. Myers, and J. Polchinski, Phys. Rev. D **46**, 2527 (1992); **46**, 2538 (1992).